W. Leterme, J. Beerten, D. Van Hertem, "Nonunit protection of HVDC grids with inductive dc cable termination," IEEE *Transactions on Power Delivery*, vol. 31, no. 2, pp. 820-828, Apr. 2016.

Digital Object Identifier: 10.1109/TPWRD.2015.2422145

URL:
http://ieeexplore.ieee.org/xpl/articleDetails.jsp?arnumber=7084157

Non-unit protection of HVDC grids with inductive dc cable termination

Willem Leterme, *Graduate Student Member, IEEE*, Jef Beerten, *Member, IEEE,* and Dirk Van Hertem, *Senior Member, IEEE*

***Abstract*—This paper deals with non-unit protection of HVDC grids by proposing a set of parameters that characterizes the open protection zones together with an efficient method to determine the thresholds on these parameters. Selective HVDC grid protection schemes must detect and discriminate faults within the first milliseconds of the fault transient and consequently differ considerably from existing ac protection schemes. Due to the accompanying speed requirement, primary protection is expected to be based on open protection zones as communication delay impedes fast operation. In the paper, the principles of the non-unit protection scheme are developed based on reflection of a traveling wave at an inductive termination. Next, the method to obtain the protection scheme thresholds is elaborated. The method accurately calculates the thresholds for HVDC grids with an arbitrary topology. A sensitivity analysis of these thresholds towards grid and fault parameters demonstrates the applicability of the proposed protection scheme in cable-based HVDC grids with inductive cable termination. The results obtained with the reduced grid model are validated by comparison against simulations using a detailed model implemented in PSCAD.**

***Index Terms*—HVDC grid, non-unit protection, open protection zone, power system fault, power system protection, VSC HVDC**

I. Introduction

VOLTAGE Source Converter High Voltage Direct Current (VSC HVDC) enables transport of bulk power over long distances. Moreover, it is the most economically viable option to connect remote offshore wind farms to the mainland ac grid. In light of these developments meshed HVDC grids gain increased attention because of higher reliability of power transfer [1], [2]. A key factor for the reliability of such a grid is a protection system that minimizes the impact of faults and ensures safe operation at all time [3].

A large scale meshed HVDC grid requires selective protection at the dc side using fast dc breakers. For selective HVDC grid protection, the dc breakers divide the HVDC grid into protection zones, similar to current ac grid protection [4]. In case of a dc fault, only the zone containing the fault is isolated, which limits the impact of the fault on the HVDC grid [5]. Alternative options for HVDC grid protection make use of converter ac breakers or converters with fault blocking capability to interrupt the dc fault current, after which dc disconnectors isolate the fault in the HVDC grid [6]. However, these protection methods cause extended outage of the full HVDC grid for dc faults, which confines their applicability to small systems.

The most stringent requirement for a selective dc protection system is speed of operation, with fault clearing times typically in the order of several milliseconds [7]. This is due to the dc fault current characteristics, which show a high rate of rise and large steady-state value [8]. The fault must therefore be cleared in a timely manner to avoid damage to the sensitive power electronic equipment and to keep the fault current below the maximal interruptible current of dc breakers. Inductors in series with the breakers are needed to extend the time for fault clearing, however the timeframe remains within several milliseconds [9]. Hence, fast primary protection for the HVDC grid is likely to be based on nonpilot protection with open protection zones [10]. Communication delay restricts the use of pilot protection to backup protection or high impedance faults, where time constraints are less stringent [11].

Because of the required speed of operation, fault detection and discrimination must occur during the transient phase of the dc fault. Consequently, HVDC grid protection differs considerably from ac grid protection, which uses the fundamental frequency component of the fault current and voltage [12]. On the contrary, the transient phase of the fault is characterized by traveling wave behavior [13]. Dc line protection based on traveling waves is already applied for point-to-point line commutated converters (LCC) HVDC, where undervoltage and voltage and current derivative are used to detect low impedance dc line faults [14], [15].

Preferably, power system protection settings are insensitive to changes in system conditions, which is the case for distance protection in ac systems [4]. This insensitivity is a main challenge for new HVDC grid protection schemes, due to the uncertainty of various parameters. First, the HVDC grid topology is not yet determined and furthermore can change during normal operation [16]. Second, the inductors in series with the breakers largely influence fault behavior in the millisecond scale. The size of these inductors is mainly determined by constraints imposed by power electronics, and can change with HVDC grid development [17]. Therefore, these uncertainties must be incorporated in the design of a new HVDC grid protection scheme to ensure general applicability.

In the literature, several protection schemes for meshed HVDC grids have been proposed. In earlier works, these

W. Leterme, J. Beerten, and D. Van Hertem are with KU Leuven, Belgium (EnergyVille/Electa research group, Electrical Engineering Department ESAT, Kasteelpark Arenberg 10 (PB2445), 3001 Heverlee).

The work of W. Leterme and J. Beerten is supported by a research grant of the Research Foundation-Flanders (FWO).

Contact: willem.leterme@esat.kuleuven.be, jef.beerten@esat.kuleuven.be, dirk.vanhertem@esat.kuleuven.be

schemes are mainly using the current magnitude and its derivative, due to large fault currents supplied by dc capacitors of two-level converters [18], [19]. These schemes thus assume dc capacitors at each terminal that allow to divide the grid into different protection zones. However, this assumption is not valid for HVDC grids with modular multilevel converters (MMCs), where dc capacitors are distributed within the submodules. The discharge of the submodule capacitors is limited by the arm reactors and can be stopped by blocking the converter IGBTs [20]. Furthermore, the dc breakers' series inductors limit the applicability of these earlier schemes in future HVDC grids. Protection schemes that use series reactors to split the grid into different zones have been proposed. In [21], the protection scheme makes use of wavelet transform of voltage magnitude and voltage and current derivative. The voltage derivative criterion has been used in [22] as a backup for a current differential protection scheme. However, both papers use extensive time domain simulations to determine the protection thresholds for only a specific small scale test system. A generalized method for determining protection thresholds in large scale HVDC grids is still missing.

In this paper, a non-unit protection scheme for selective HVDC grid protection is developed. First, the paper proposes a set of parameters that characterizes the open protection zones. The non-unit protection scheme makes use of inductive termination of the cables to divide the grid into different zones. Second, a method to determine the thresholds on these parameters is provided. This method makes use of a reduced HVDC grid model, which enables efficient calculation for large scale HVDC grids with an arbitrary topology while maintaining high accuracy Third, the validity of the proposed protection scheme in a dynamic and continuously evolving HVDC grid is analyzed. This is done by a sensitivity analysis of the protection thresholds for various parameters such as grid topology, cable length and series inductor size.

The paper is structured as follows: Section II provides an overview of the HVDC grid transient phenomena and traveling waves on which the non-unit protection scheme must act. Section III presents the protection principles on which the non-unit protection scheme is based. Section IV introduces the reduced grid model for determining the protection thresholds and provides a discussion on the results of the sensitivity analysis. In Section V, a case study in PSCAD is performed to demonstrate the validity of the protection thresholds obtained by the reduced grid model.

II. DC FAULT TRANSIENT PHENOMENA

Due to the limited time available for fault clearing, fault detection and discrimination must occur during the dc fault transient. This is illustrated by Fig. 1a, which shows a part of an HVDC grid with dc cables terminated by inductors at each end. A relay and breaker at location R are shown for the dc cable in the middle. For non-unit protection, this relay must discriminate internal faults (F_1) from external faults (F_2, F_3) using local measurements.

After a fault, the voltage and current measured at the cable termination can initially be described by traveling waves. This

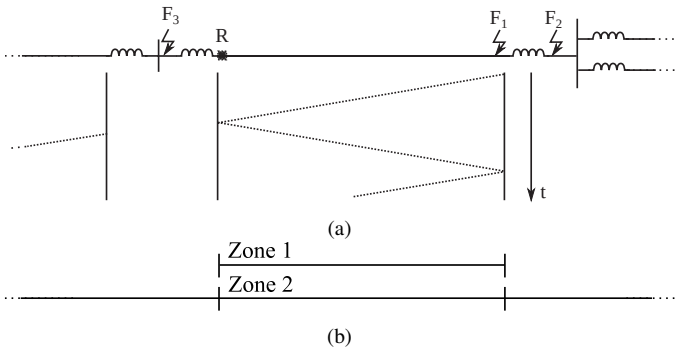

Fig. 1. Faults on a DC cable within a grid and lattice diagram for fault F_1 or F_2 (a) and protection zones for relay R (b).

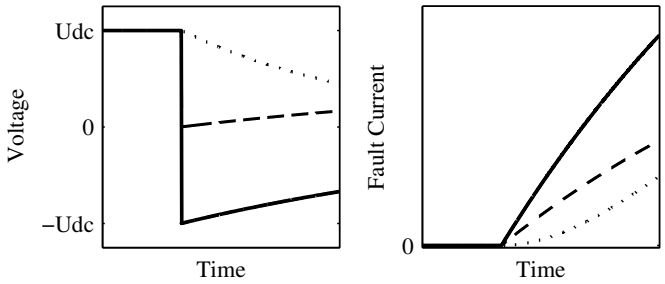

Fig. 2. Voltage and current for fault wave reflected at inductive terminal (solid line: F_1, $R_\mathrm{f} = 0\ \Omega$, dashed line: F_1, $R_\mathrm{f} = Z_c/2$, dotted line: F_2, $R_\mathrm{f} = 0\ \Omega$).

is visualized for faults F_1 or F_2 by the Bewley lattice diagram shown in Fig. 1a. The wave created at the fault location travels to the cable termination, where it is partly reflected back to the fault location and partly transmitted to the rest of the grid. In course of time, reflected waves from other terminals in the network are superposed. For the reflection of the first incident wave from faults F_1 and F_2, the voltage and current measured at R, respectively U_R and I_R, can be described as follows:

$$U_\mathrm{R} = (1 + \Gamma) \cdot A \cdot U_\mathrm{fault}, \tag{1}$$

$$I_\mathrm{R} = (1 - \Gamma) \cdot A \cdot I_\mathrm{fault}, \tag{2}$$

where Γ is the reflection coefficient, determined by the cable characteristic impedance and the cable termination impedance [13], A represents the wave propagation over the cable, determined by cable parameters and cable length [23], and U_fault and I_fault are the voltage and current wave on the cable at the location of the fault, determined by fault location and impedance. The reflection of the first incident wave is thus determined only by the faulted cable characteristics and local cable termination impedance.

1) Voltage and current wave at the fault location: U_fault or I_fault are the only variables in (1) and (2) that distinguish forward faults at the end of the cable, F_1, from faults behind the series inductor, F_2. The worst case for discriminating both faults is a high resistance fault at F_1 and a solid fault at F_2. To simplify the analysis at this stage, the fault F_1 is considered to occur before the cable end. If a fault occurs, the voltage at the fault location changes from the pre-fault voltage, U_0 to zero.

This voltage change, $-U_0$, is divided over the fault resistance and the cable according to

$$U_{\text{fault,F1}} = \frac{Z_\text{c}/2}{R_\text{f} + Z_\text{c}/2}(-U_0), \tag{3}$$

in which R_f is the fault resistance and the factor 1/2 accounts for the fact that the fault resistance is in series with the cable impedances at both sides. For a solid fault at F_2, a similar relationship is found between the pre-fault voltage U_0 and the voltage wave at the cable $U_{\text{fault,F2}}$. In this case, the voltage change -U_0 at the fault location is divided over the cable and the inductor:

$$U_{\text{fault,F2}} = \frac{Z_\text{c}}{sL + Z_\text{c}}(-U_0), \tag{4}$$

in which L is the inductor value and Z_c is the characteristic impedance. The difference between (3) and (4) lies in the pole caused by the series inductor L. The inductor filters out high frequencies of $U_{\text{fault,F2}}$, whereas the fault resistance R_f provides an overall damping of the amplitude of $U_{\text{fault,F1}}$.

2) Reflection at an inductive termination: The reflection coefficient Γ relates the reflected wave to the incident wave. For a purely inductive cable termination, considering a solid fault on a lossless line, the time domain counterparts of (1) and (2) are given by [24]:

$$\begin{aligned} i_R =& 2(1 - e^{-t/(L/Z_c)})i_{\text{fault}} \\ u_R =& 2e^{-t/(L/Z_c)}u_{\text{fault}}, \end{aligned} \tag{5}$$

where u_{fault} is the amplitude of the incident voltage wave and $i_{\text{fault}} = u_{\text{fault}}/Z_c$. For a lossless cable, the voltage measured at the terminal u_R is at $t = 0$ twice the incident voltage wave. The current i_R is at $t = 0$ zero, whereas it increases with a time constant defined by the ratio L/Z_c.

Fig. 2 shows the reflection of the first incident voltage and current wave at relay R for faults F_1 (0 and $Z_\text{c}/2$ Ω) and F_2 (0 Ω). The cable is assumed to be lossless, which leads to a steep crest in the voltage for faults at location F_1. The difference between faults F_1 and F_2 can be clearly seen, as the voltage derivative of F_2 is much lower in magnitude.

III. Non-unit protection scheme

This section develops the principles for the non-unit protection scheme. The protection scheme follows a two-stage approach. In the first stage, the protection algorithm is started by fault detection. Thereafter, the faulted zone is located by fault discrimination in the second stage [11]. Section IV provides the method for determining the protection thresholds and the visualization of the protection zones.

A. Protection zones

Fig. 1b shows the first and second zone for the proposed non-unit protection scheme. The first zone or zone of primary protection is bounded by the series inductors terminating the protected cable. The second zone, for which the relay must provide backup protection, covers the first zone and parts of the surrounding cables. The aim of this paper is to provide protection principles to discriminate between first and second zone. The boundaries of the second zone are not considered.

B. Fault detection

The protective algorithm is initiated by a starting function that is used to detect dc side faults. Beside the required speed of operation, the main requirement for the starting function is dependability as the protective algorithm must be initiated for every possible fault (i.e. for faults in the first as well as the second zone). Fundamentally, faults are characterized by a decreasing voltage and an increasing current magnitude. As discussed in Section II, the voltage wave is largely reflected by series inductors, whereas the current only increases slowly (Fig. 2). Therefore, faults can be detected swiftly by using an undervoltage criterion to discriminate normal operation from faults:

$$U_\text{R} < U_{<,\text{s}}. \tag{5}$$

In (6), the threshold $U_{<,\text{s}}$ must be set to discriminate between faults and normal operation. The time for fault detection t_{det} depends on the voltage derivative. First zone faults (F_1) are detected faster than second zone faults (F_2), as the voltage drop for second zone faults is slower (Fig. 2).

C. Fault discrimination

In the second stage the protection zone in which a fault occurs must be identified to guarantee selective tripping. Security is important in this stage because a breaker must only be tripped instantly for faults occuring in the first zone.

Considering Figs. 1a and 2, the discrimination of forward faults F_1 and F_2 is most clear in the voltage. As indicated in Section II, the difference between both faults is in the high frequency region. For the transient of fault F_1, high frequencies are present but equally attenuated by the fault resistance. For the fault transient of F_2 high frequencies are filtered out due to the inductor. Therefore, the first proposed criterion to discriminate forward faults F_1 and F_2 is based on voltage derivative.

Basing fault discrimination purely on the voltage derivative criterion is not secure due to interference of measurement errors and noise. Moreover, considering digital sampling, the number of samples which show a high voltage derivative is limited especially for close faults that are only slightly attenuated by the cable. To overcome this problem, an undervoltage criterion is proposed. The undervoltage criterion is achieved by monitoring the voltage after a defined period of time t_{discr} after fault detection. This criterion must be considered independently from the voltage derivative criterion, as both criteria are possibly not satisfied at the same time (e.g. as in Fig. 2).

The voltage does not contain information on the direction of the fault and accordingly does not allow to discriminate forward and backward faults. Therefore, the current derivative is additionally used to discriminate between forward and backward faults. The sign of the current derivative determines the fault direction; a positive or negative sign indicates a forward or backward fault respectively. The first and second

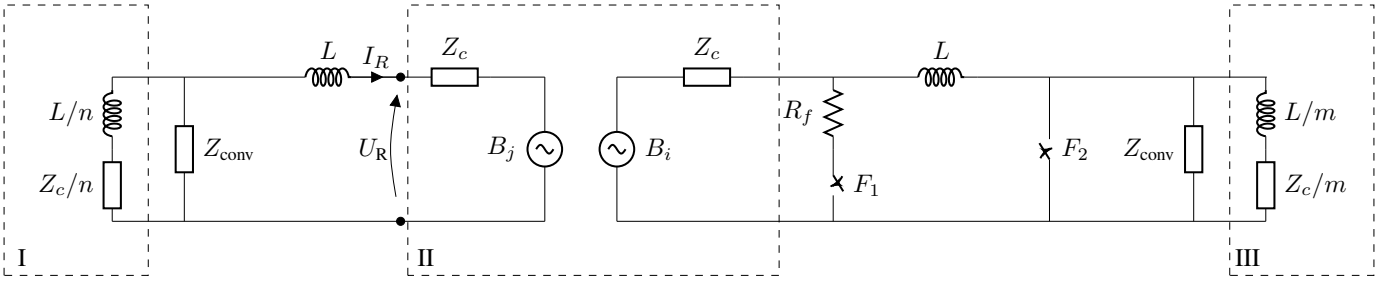

Fig. 3. Reduced grid model to evaluate the fault transient for faults F_1 and F_2.

zone can now be defined using both voltage and current criteria:

$$\text{First zone} \begin{cases} \frac{dU_{\text{R}}}{dt} < \left(\frac{dU}{dt}\right)_{<,1} \\ U_{\text{R},t_{\text{discr}}} < U_{<,1} \\ \frac{dI_{\text{R}}}{dt} > 0 \end{cases}, \tag{6}$$

$$\text{Second zone} \begin{cases} \frac{dU_{\text{R}}}{dt} > \left(\frac{dU}{dt}\right)_{<,1} \\ U_{<,1} < U_{\text{R},t_{\text{discr}}} < U_{<,\text{s}} \end{cases}.$$

The total time for the protection algorithm consists of the fault detection time t_{det} and the fault discrimination time t_{discr}. The fault discrimination time t_{discr} must be fixed to a small value as also for second zone faults the voltage keeps decreasing in time (Fig. 2).

IV. Protection thresholds

This section deals with the determination of the protection thresholds for the principles proposed in the previous section. For this purpose, a reduced grid model is first developed. The reduced model can be used for fault analysis and determination of the thresholds of (7). At last, a sensitivity analysis on these thresholds is performed.

A. Reduced grid model

The focus of the reduced grid model lies on fault detection and discrimination, thus it needs to be accurate for the first milliseconds of the fault transient. The model is described in the Laplace domain, after which an inverse Laplace transform can be performed to obtain a time domain response.

1) Cable model: The cables are modeled by a frequency-dependent distributed parameters model to incorporate traveling wave effects, as shown in Fig. 3(II) [25]. The propagation of waves on cables is described by two parameters; the propagation constant γ and the characteristic impedance Z_c. The voltage source B_i relates cable end i to the other j [26]:

$$B_i = AF_j = e^{-\gamma l}F_j, \tag{7}$$

where F_j is the forward voltage wave at end j and l is the length of the cable section. A reflects the voltage transfer from one end to the other, which is characterized by attenuation and a time delay. If this time delay is larger than the timeframe of interest, the voltage sources become short circuits.

By fitting the parameters A and Z_c using rational functions in the frequency domain, a linearized cable model is obtained. In this paper, these parameters are obtained via the PSCAD cable constants routine which makes use of Vector Fitting and dc correction techniques [27–30].

2) Converter model: The converter topology considered in this study is the modular multilevel converter (MMC). The converter fault contribution can be split into a capacitive discharge phase and an AC infeed phase. As only the first milliseconds are of interest for the protection algorithm, only the capacitive discharge phase of the converter fault contribution must be taken into account. The discharge of the submodule capacitors can be approximated by an equivalent capacitance that represents the total capacitance of all inserted submodules at the moment of the fault. This capacitance is in series with an equivalent inductance and resistance, which represent the arm reactors and the resistance of the power electronics. The parameters of this equivalent RLC-model are readily derivable from the converter topology, as discussed in greater detail for the half-bridge MMC in [31]. Following this approach, the converter is modeled by an impedance Z_{conv}:

$$Z_{\text{conv}} = R_{\text{conv}} + sL_{\text{conv}} + \frac{1}{sC_{\text{conv}}}, \tag{8}$$

in which R_{conv}, L_{conv} and C_{conv} are the converter equivalent resistance, inductance and capacitance in the RLC-model.

3) Grid Model: Fig. 3 shows the resulting reduced grid model to simulate the transient phase for faults in a HVDC grid. The cable covered by the relay R (II) is terminated by inductors at each side, whereas the measurements I_{R} and U_{R} are at the cable side of the inductor. At each termination, a converter is modeled by its equivalent impedance Z_{conv}. The cables connected to the remainder of the grid (I and III) are modeled by the characteristic impedance Z_c in series with an inductor L. This assumes that traveling waves reflected by remote terminals only impact the fault transient outside the time frame of interest. For cable systems, this is a reasonable assumption as propagation speeds are approximately half the speed of light. The model is thus valid for cable lengths as short as 75 km if only the first millisecond of the transient is used for fault detection and discrimination.

The cables are assumed to have the same characteristic impedance Z_c. Therefore, the other cables departing from the terminals adjacent to the faulted cable can be modeled as one parallel equivalent branch, with an impedance n or m times smaller. It should be noted that when there are no other cables departing to the rest of the grid (n or m equal to zero), parts I and II in Fig. 3 should be omitted.

In this form, the grid model is directly applicable for the analysis of pole-to-ground faults in an asymmetric monopolar system or bipolar system, considering solid grounding at each terminal. The analysis using this grid model can be extrapolated to pole-to-pole faults in a symmetric monopolar system, considering appropriate adaptation of the pole-to-ground voltages and impedances to their pole-to-pole equivalents. To study different grounding schemes in asymmetric monopolar or bipolar systems [32], the grounding impedance and metallic return cable should be included in the model. These impedances would appear in series with the converter impedance.

4) Time domain response: As all components in the reduced grid model are linear, the model can be described in the Laplace domain. To obtain a time domain response after a fault, the transfer function of the voltage and current at the fault location to the relay location is first derived from the model. Subsequently, a step input with magnitude $-U_0$ is applied at the fault location. The inverse Laplace transform of the resulting system leads to the time demain response at relay R. The simulations have been performed in Matlab.

B. Determination of thresholds

Fig. 4 shows the locus of the voltage and voltage derivative of the voltage U_{R} for faults F_1 and F_2. This figure is obtained using the model depicted in Fig. 3 and the parameters enlisted in Tables I and II. For this case, the system configuration is asymmetric monopolar with pole-to-ground voltage 320 kV. The faults F_1 and F_2 are pole-to-ground faults. The fault F_1 has a resistance of 10 Ω, which is approximately $Z_c/2$. Fig. 4 thus depicts similar waveforms as Fig. 2, but now also includes cable attenuation. The cable attenuates high frequencies, which rounds off the steep crests in Fig. 2. In Fig. 4, the starting criterion and discrimination criteria based on the voltage are also plotted.

1) Fault detection: The undervoltage threshold discriminates faulted operation from normal operation. The threshold can in theory be set to the minimal allowed voltage during normal operation. As an example, the undervoltage threshold has been set to 85% of the nominal voltage (320 kV) in Fig. 4.

2) Fault discrimination: For the discrimination stage, the thresholds for the voltage derivative and undervoltage criterion can in theory be set to the minimum values occuring for a solid fault at F_2, as shown in Fig. 4:

$$\left(\frac{dU}{dt}\right)_{<,1} = \min\left(\frac{dU_{\mathrm{F2}}}{dt}\right) \tag{9}$$

$$U_{<,1} = U_{\mathrm{F2},t_{\mathrm{det}}+t_{\mathrm{discr}}}, \tag{10}$$

in which U_{F2} is the voltage measured at the relay for a fault F_2 at the remote bus. Fig. 4 visualizes these thresholds by showing the voltage-voltage derivative pairs in function of time. The dot markers indicate samples taken at a sampling frequency of 100 kHz, starting from fault detection. For faults F_1, the density of the markers indicates that only a limited amount of samples is available at which the magnitude of the voltage derivative is high. The time t_{discr} for the undervoltage criterion has been taken as 100 μs, which corresponds to the tenth sample after fault detection, indicated by the square marker. A longer time t_{discr} or a lower sampling frequency leads to a less sensitive protection scheme.

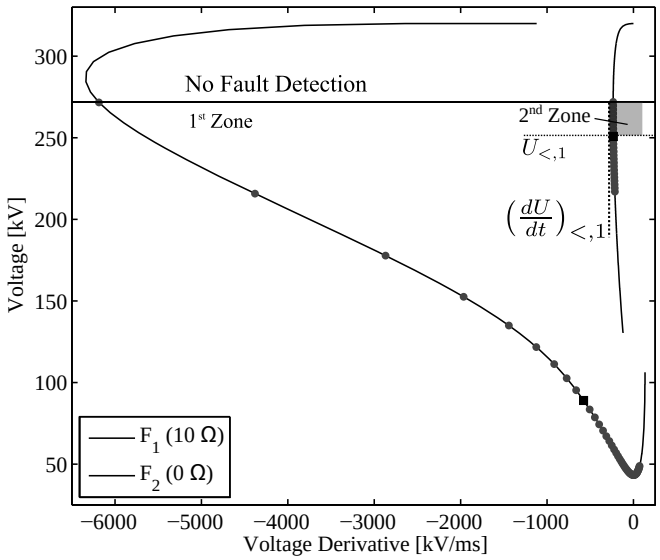

Fig. 4. Protection zones and thresholds in the voltage/voltage derivative plane.

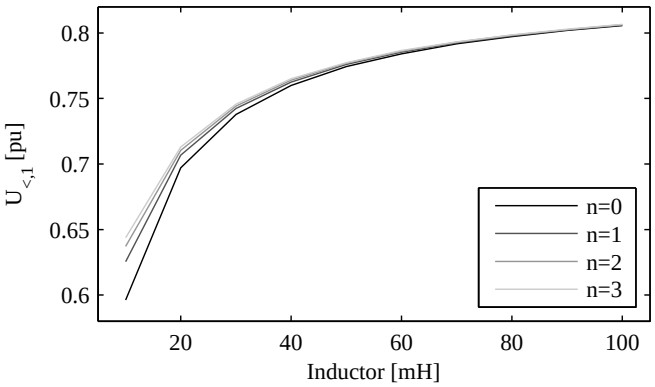

Fig. 5. Voltage threshold in function of inductor value and grid topology.

C. Sensitivity analysis

To demonstrate the validity of the protection scheme, a sensitivity analysis is performed towards protection thresholds and sensitivity towards fault resistance. The considered parameters are series inductor value L, grid topology at bus (by varying the number of cables n in Fig. 3(I)) and cable length l.

1) Protection thresholds: The thresholds for the undervoltage and voltage derivative criterion are shown in Figs. 5 and 6 for various inductor values and grid topologies. The selected cable length is 200 km. Both undervoltage and voltage derivative criterion show the same trend when changing the inductor value. This is due to the almost constant voltage derivative of faults in the second zone (Fig. 4).

The variation of the thresholds with inductor value is limited and decreases with increasing inductor value. Moreover, the maximum frequency in a voltage wave at R for a fault F_2 is

TABLE I
GRID AND CONVERTER PARAMETERS

Dc voltage (pole-to-ground) $U_{\text{dc,ptg}}$	320 kV
Inductor Size L	25 mH
Cable length l	200 km
Number of cables at bus n	2
Number of cables at bus m	2
F_1 resistance	10 Ω
F_2 resistance	0 Ω
C_{conv}	175.8 μF
L_{conv}	0.0383 mH
R_{conv}	0.295 Ω

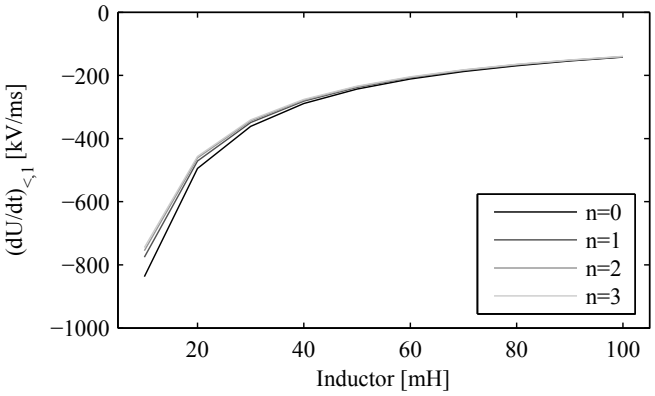

Fig. 6. Voltage derivative threshold in function of inductor value and grid topology.

determined by the cable attenuation. For large inductors, the filtering effect of the inductor is thus cancelled out by cable attenuation. The effect of grid topology (shown by varying the number of cables n in part I of the grid of Fig. 3) is limited and also diminishes with increasing inductor value. As an important consequence, the inductors decouple the faulted line from the remainder of the grid in terms of traveling waves. The sensitivity analysis thus shows that the series inductors enable to determine protection thresholds that are almost fully independent from grid topology.

2) Fault resistance: To investigate the sensitivity of the protection scheme towards fault resistance, the maximum fault resistance for faults F_1 that can be discriminated from solid faults F_2 is plotted as function of inductor value and cable length in Fig. 7. Increasing the fault resistance diminishes the wave amplitude of $U_{\text{fault,F1}}$ for all frequencies, as shown in (3). Consequently, the voltage derivative as seen by the relay diminishes and the voltage drop is lower, leading the loci of the voltage/voltage derivative closer to the second zone (Fig. 4). Discrimination of faults F_1 from a solid fault $F2$ becomes more difficult for larger fault resistances of F_1.

For a given cable length, the maximal fault resistance increases with increasing inductor value. The cable length also influences the maximal fault resistance. This is due to the attenuation of the high frequencies of a traveling wave on a cable. The longer the cable is, the more frequencies are attenuated. Therefore, the filtering effect of the inductor at the end of the cable relatively diminishes with respect to the

TABLE II
CABLE PARAMETERS

	Outer radius [mm]	ρ [Ωm]	ϵ_{rel} [-]	μ_{rel} [-]
Copper Core	19.5	1.7e-8	-	1
XLPE Insulation	48.7	-	2.3	1
Lead Sheath	51.7	2.2e-7	-	1
XLPE Insulation	54.7	-	2.3	1
Armor	58.7	1.8e-7	-	10
XLPE Insulation	63.7	-	2.3	1

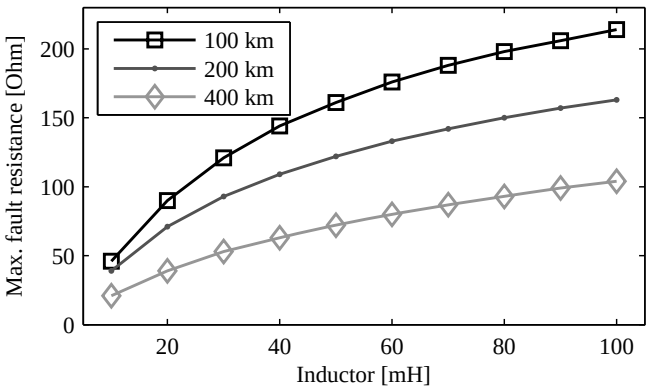

Fig. 7. Maximum fault resistance for given thresholds in function of inductor value and three cable lengths l.

filtering effect of the cable with increasing cable length.

V. CASE STUDY

In this section, a case study using a detailed test system implemented in PSCAD is performed to demonstrate the validaty of the results obtained by the reduced grid model.

A. Test System

The test system for the case study is the four bus meshed test system described in [33] and shown in Fig. 8. This four bus test system represents an offshore meshed HVDC grid connecting two offshore wind farms to two onshore ac networks.

The converters in the model are half-bridge modular multilevel converters modeled by a continuous model with IGBT blocking capability [34]. The nominal power is 900 MW for converters 1 to 3 and 1200 MW for converter 4. The converter IGBTs are blocked if the current exceeds a value of 2.2 kA. An inductor of 10 mH is inserted between converter and dc bus to filter out converter noise. The cable geometry and material parameters are the same as in Table II, whereas cable lengths are indicated in the Fig. 8.

The system of [33] has a symmetric monopolar configuration with a pole-to-pole voltage of 640 kV. The faults that are applied in this system are pole-to-pole faults with a connection to ground, whereas the fault resistance has been equally divided between positive and negative pole. For the simulations of the detailed model, the positive pole-to-ground voltage and the positive pole-to-ground resistance are shown. This enables a direct comparison of the results of the simulations of the detailed model against the reduced grid

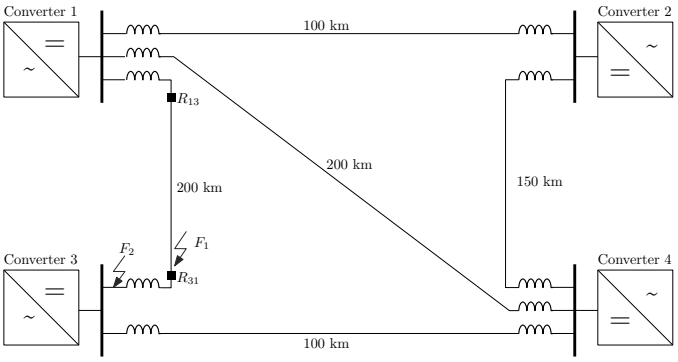

Fig. 8. Four bus test system with faults indicated.

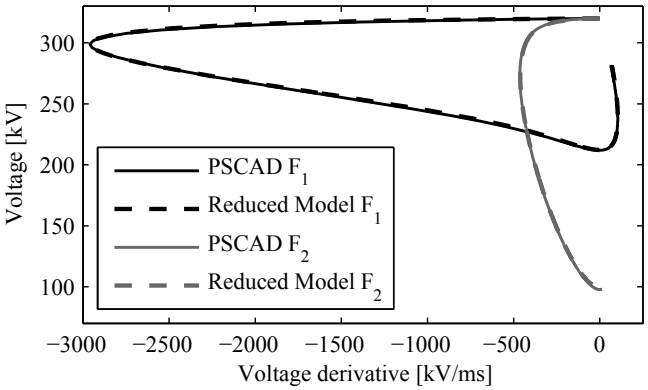

Fig. 9. Comparison of results of reduced grid model with PSCAD model for faults F_1 (60 Ω) and F_2 (0 Ω).

model with converter parameters given in Table Iand pole-to-ground voltage of 320 kV. The converter parameters have been calculated for the converters in [31] and transformed to parameters for the equivalent asymmetric system.

Hybrid HVDC breakers in series with an inductor are included at the end of each cable. These breakers insert a countervoltage after a certain delay due to opening of the mechanical switch [35]. To incorporate these effects, the breakers are modeled as an ideal switch that opens with a delay of 2 ms, in parallel with a surge arrester that inserts a voltage of 480 kV [9]. The size of the series inductors is determined by the current interruption capability and interruption time. These values are fixed to 20 mH and 40 mH, respectively corresponding to a fault current rate of rise of 10 kA/ms and 6 kA/ms.

As starting situation, converters 1 and 2 both inject 700 MW whereas converters 3 and 4 are in rectifying mode, respectively absorbing 600 and 800 MW. The faults studied in the circuit are faults F_1 and F_2, respectively occuring at the end of cable 13 and at bus 3.

B. Comparison with detailed model

Fig. 9 shows the voltage and voltage derivative at relay R_{13} for faults F_1 and F_2 (fault resistances of 60 and 0 Ω), obtained by the reduced grid model and the detailed PSCAD simulation. Qualitatively, the waveforms obtained by both models correspond well. Table III shows a comparison of the thresholds predicted by the reduced model with the ones obtained by the detailed model. The relative errors between thresholds obtained by both models do not exceed 0.5%, which confirms the suitability of the reduced model to determine protection thresholds.

Table III further enlists the protection thresholds for both models for the 40 mH case. This case also supports the suitability of the reduced model to determine the protection thresholds, with relative errors below 0.2% compared to the detailed model.

C. Time Domain Results

The proposed protection scheme has been fully implemented in PSCAD for testing with the detailed model. For this test, a 20 mH series inductor is used. A fault F_1 of 60 Ω is applied at the end of cable 13 to analyze the protection scheme for dependability, as this is the worst case for detection. A solid fault at bus 3 is applied to check the security of the protection of cable 13.

TABLE III
THRESHOLDS FOR REDUCED GRID MODEL AND PSCAD MODEL

Inductor	Threshold		Red. Model	PSCAD	Rel. error
20 mH	$U_{<,1}$ [pu]		0.7110	0.7110	0.0042%
	$\left(\frac{dU}{dt}\right)_{<,1}$	[kV/ms]	-461.4483	-463.5521	0.4539%
40 mH	$U_{<,1}$ [pu]		0.7640	0.7639	0.0160%
	$\left(\frac{dU}{dt}\right)_{<,1}$	[kV/ms]	-278.0237	-278.4370	0.1485%

Fig. 10 shows the voltages and currents at relays R_{13} and R_{31} for fault F_1 of 60 Ω (Fig. 8). The fault occurs at 2 ms and directly affects the voltage and current at relay R_{13}. The fault is detected immediately, t_{det} is 0, and discriminated after the fixed time t_{discr} of 100 μs. Due to the breaker delay fault clearing starts 2 ms later, causing the voltage to increase and the current to decrease at 4 ms. By contrast, it takes 1.09 ms for the fault to reach relay R_{13} due to the traveling wave delay over the cable. The time for fault detection, t_{det} is 10 μs. Together with the fault discrimination time of 100 μs, the breaker is tripped 0.11 ms after the fault reaches the relay. In conclusion, the total time until fault current interruption is 2.11 ms and the fault is cleared by the breaker associated to R_{13} 3.2 ms after fault inception.

For the fault F_2 at bus 3, the protections that are triggered are shown in Table IV. Relay R_{13} sees a forward fault but the undervoltage and voltage derivative criterion indicate a fault outside the first protection zone. For relay R_{31}, closest to the fault, the directional criterion based on the current derivative inhibits tripping of the breaker.

VI. CONCLUSION

The non-unit protection scheme for cable-based HVDC grids makes use of voltage magnitude and derivative to discriminate forward faults and current derivative to discriminate forward from backward faults. By plotting the locus of the voltage magnitude and derivative, the open protection zones

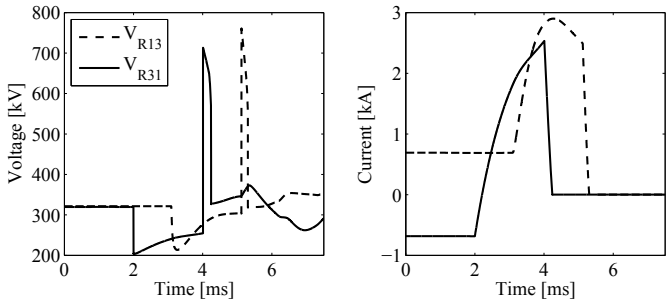

Fig. 10. DC fault voltages and currents for a pole-to-pole fault F_1 of 60 Ω.

TABLE IV
PROTECTIONS TRIGGERED

Relay	F_1 (60 Ω) $U_{<,1}$	F_1 (60 Ω) $\left(\frac{dU}{dt}\right)_{<,1}$	F_1 (60 Ω) Dir.	F_2 (0 Ω) $U_{<,1}$	F_2 (0 Ω) $\left(\frac{dU}{dt}\right)_{<,1}$	F_2 (0 Ω) Dir.
R_{13}	1	1	1	0	0	1
R_{31}	1	1	1	1	1	0

can be clearly determined in the voltage/voltage derivative plane. These protection zones are defined based on the inductive termination of the cables. Furthermore, an efficient method for determining the protection thresholds is provided. This method is obtained by reducing the HVDC grid model to only the faulted cable and its adjacent terminals.

A sensitivity analysis of the protection thresholds demonstrates the validity of the protection scheme for a large range of parameters. First, the protection thresholds are insensitive towards grid topology, due to the presence of series inductors which largely reflect the voltage wave. Second, the protection scheme remains valid even for low series inductor values or large cable lengths although sensitivity of the protection scheme towards fault resistance decreases. Nonetheless, faults with a significant fault resistance can be discriminated from second zone faults even for low inductor sizes.

Finally, a comparison of thresholds obtained with the reduced model against thresholds obtained by simulation with a detailed model in PSCAD justifies the use of the reduced model to determine protection thresholds. A case study in PSCAD furthermore shows that the proposed protection scheme can reliably detect and discriminate faults in the HVDC grid.

REFERENCES

[1] J. De Decker and P. Kreutzkamp, "Offshore Electricity Grid Infrastructure in Europe, Final Report," OffshoreGrid, Tech. Rep., 2011.

[2] D. Van Hertem and M. Ghandhari, "Multi-terminal VSC HVDC for the European supergrid: Obstacles," *Renewable and Sustainable Energy Reviews*, vol. 14, no. 9, pp. 3156 – 3163, 2010.

[3] V. Akhmatov, M. Callavik, C. Franck, S. Rye, T. Ahndorf, M. Bucher, H. Muller, F. Schettler, and R. Wiget, "Technical guidelines and prestandardization work for first HVDC grids," *IEEE Trans. Power Del.*, vol. 9, no. 1, pp. 327 – 335, Feb. 2013.

[4] P. Anderson, *Power System Protection*. Hoboken, NJ, USA: J. Wiley & Sons, 1998.

[5] Alstom, *Network Protection and Automation Guide*. Alstom Grid, 2011.

[6] L. Tang and B. Ooi, "Locating and isolating dc faults in multi-terminal dc systems," *IEEE Trans. Power Del.*, vol. 22, no. 3, pp. 1877–1884, Jul. 2007.

[7] D. Van Hertem, M. Ghandhari, J. Curis, O. Despouys, and A. Marzin, "Protection requirements for a multi-terminal meshed DC grid," in *CIGRE 2011 Bologna Symp.*, Bologna, Italy, 13-15 Sep. 2011, 8 p.

[8] M. Bucher and C. Franck, "Contribution of fault current sources in multiterminal HVDC cable networks," *IEEE Trans. Power Del.*, vol. 28, no. 3, pp. 1796–1803, 2013.

[9] J. Häfner and B. Jacobson, "Proactive Hybrid HVDC Breakers: A key innovation for reliable HVDC grids," in *CIGRÉ Bologna Symp.*, Bologna, Italy, 13- 15 Sep. 2011, 8 pages.

[10] S. Horowitz and A. Phadke, *Power System Relaying*. Hoboken, NJ, USA: J. Wiley & Sons, 2008.

[11] G. Ziegler, *Numerical Distance Protection*. Erlangen, Germany: Siemens, 2006.

[12] A. Phadke and J. Thorpe, *Computer Relaying for Power Systems*. Hoboken, NJ: J. Wiley & Sons, 2009.

[13] L. van der Sluis, *Transients in Power Systems*. Hoboken, NJ, USA: John Wiley & Sons, Inc., 2001.

[14] D. Naidoo and N. Ijumba, "HVDC line protection for the proposed future HVDC systems," in *IEEE PowerCon 2004*, vol. 2, 21-24 Nov. 2004, pp. 1327–1332 Vol.2.

[15] K. Padiyar, *HVDC Power Transmission Systems, Technology and System Interactions*. Delhi, India: New Age International Publishers, 1990.

[16] M. Bucher, R. Wiget, G. Andersson, and C. Franck, "Multiterminal HVDC networks - What is the preferred topology?" *IEEE Trans. Power Del.*, vol. 29, no. 1, pp. 406–413, Feb. 2014.

[17] F. Deng and Z. Chen, "Design of protective inductors for HVDC transmission line within dc grid offshore wind farms," *IEEE Trans. Power Del.*, vol. 28, pp. 75–83, Jan. 2013.

[18] L. Tang, "Control and protection of multi-terminal DC transmission systems based on voltage-source converters," Master's thesis, McGill University, Montreal, Canada, 2003.

[19] J. Yang, J. Fletcher, and J. O'Reilly, "Multiterminal dc wind farm collection grid internal fault analysis and protection design," *IEEE Trans. Power Del.*, vol. 25, no. 4, pp. 2308–2318, 2010.

[20] S. Allebrod, R. Hamerski, and R. Marquardt, "New transformerless, scalable Modular Multilevel Converters for HVDC-transmission," in *Proc. IEEE PESC 2008*, Rhodes, Greece, 15-19 Jun. 2008, pp. 174–179.

[21] K. De Kerf, K. Srivastava, M. Reza, D. Bekaert, S. Cole, D. Van Hertem, and R. Belmans, "Wavelet-based protection strategy for dc faults in multi-terminal VSC HVDC systems," *IET Generation, Transmission & Distribution*, vol. 5, no. 4, pp. 496–503, April 2011.

[22] J. Descloux, "Protection contre les courts-circuits des réseaux à courant continu de forte puissance," Ph.D. dissertation, Université de Grenoble, Grenoble, France, Sep. 2013.

[23] J. Martinez-Velasco, *Power System Transients: Parameter Determination*. Boca Raton, FL, USA: CRC Press, 2009.

[24] E. W. Kimbark, "Transient overvoltages caused by monopolar ground fault on bipolar dc line: theory and simulation," *IEEE Trans. Power App. Syst.*, vol. PAS-89, no. 4, pp. 584–592, 1970.

[25] J. Marti, L. Marti, and H. Dommel, "Transmission line models for steady-state and transients analysis," in *Proc. IEEE APT '93*, Athens, Greece, 5-8 Sep. 1993, pp. 744–750.

[26] N. Watson and J. Arrillaga, *Power Systems Electromagnetic Transients Simulation*. Stevenage, UK: IET, 2003.

[27] PSCAD. (2010) EMTDC User Guide. [Online]. Available: https://hvdc.ca/knowledge-library/reference-material

[28] B. Gustavsen and A. Semlyen, "Rational approximation of frequency domain responses by vector fitting," *IEEE Trans. Power Del.*, vol. 14, no. 3, pp. 1052–1061, 1999.

[29] A. Morched, B. Gustavsen, and M. Tartibi, "A universal model for accurate calculation of electromagnetic transients on overhead lines and underground cables," *IEEE Trans. Power Del.*, vol. 14, no. 3, pp. 1032–1038, 1999.

[30] H. De Silva, A. Gole, and L. Wedepohl, "Accurate electromagnetic transient simulation of HVDC cables and overhead lines," in *IPST 2007*, Lyon, France, 4-7 Jun. 2007.

[31] W. Leterme and D. Van Hertem, "Reduced modular multilevel converter model to evaluate fault transients in dc grids," in *Proc. IET DPSP 2014*, Copenhagen, Denmark, 31 Mar.-3 Apr. 2014, 6 pages.

[32] W. Leterme, P. Tielens, S. De Boeck, and D. Van Hertem, "Overview of Grounding and Configuration Options for Meshed HVDC Grids," *IEEE Trans. Power Del.*, vol. 29, no. 6, pp. 2467–2475, Dec 2014.

[33] W. Leterme, N. Ahmed, L. Ängquist, J. Beerten, D. Van Hertem, and S. Norrga, "A new HVDC grid test system for HVDC grid dynamics and protection studies in EMTP," in *Proc. IET ACDC*, Birmingham, UK, 10-12 Feb. 2015, 7 pages.

[34] N. Ahmed, L. Ängquist, S. Norrga, and H.-P. Nee, "Validation of the continuous model of the modular multilevel converter with blocking/deblocking capability," in *Proc. IET ACDC 2012*, Birmingham, UK, 4-6 Dec. 2012, 6 pages.
[35] C. Franck, "HVDC circuit breakers: A review identifying future research needs," *IEEE Trans. Power Del.*, vol. 26, no. 2, pp. 998–1007, 2011.

Willem Leterme (S'12) was born in 1989 in Izegem, Belgium. He received the M.Sc. degree in electrical energy engineering from the University of Leuven (KU Leuven), Leuven, Belgium in 2012. Currently, he is working at KU Leuven in the research group Electa, dept. of Electrical Engineering, to obtain the Ph.D. degree. His research is funded by a PhD Fellowship of the Research Foundation - Flanders (FWO). His research interests include transient fault studies and design of protection algorithms for meshed VSC HVDC grids.

Jef Beerten (S'07–M'13) was born in Belgium in 1985. He received the M.Sc. degree in electrical engineering from the University of Leuven (KU Leuven), Leuven, Belgium, in 2008, and the Ph.D. degree in 2013, also from KU Leuven. In 2011, he was a visiting researcher at the EPS group of the Royal Institute of Technology (KTH), in Stockholm, Sweden. Currently, he is a Postdoctoral Researcher with the ESAT-ELECTA division of KU Leuven and a visiting researcher at the Norwegian University of Science and Technology (NTNU) in Trondheim, Norway. His research interests include power system control, the grid of the future and multiterminal VSC HVDC in particular. His research has been funded by a Ph.D. fellowship from the Research Foundation—Flanders (FWO). Currently, he holds a postdoctoral fellowship from the FWO. Dr. Beerten is an active member of both IEEE and CIGRÉ.

Dirk Van Hertem (S'02-SM'09) was born in 1979, in Neerpelt, Belgium. He received the M.Eng. in 2001 from the KHK, Geel, Belgium and the M.Sc. in electrical engineering from the KU Leuven, Belgium in 2003. In 2009, he received the Ph.D., also from the KU Leuven. In 2010, he was a member of EPS group at the Royal Institute of Technology, in Stockholm, Sweden, where he was the program manager for controllable power systems for the EKC^2 competence center. Since spring 2011 he is back at the University of Leuven where he is an Assistant Professor in the Electa group. His special fields of interest are power system operation and control in systems with FACTS and HVDC and building the transmission system of the future, including offshore grids and the supergrid concept. He is an active member of IEEE PES and IAS and CIGRÉ.